hydrology

MDPI

Article

A Sensitivity Study of Vertical and Horizontal River–Aquifer Exchange and Implications for Flood Attenuation

Gadadhara de Figueiredo Ferraz * and Tamás Krámer

Department of Hydraulic and Water Resources Engineering, Budapest University of Technology and Economics, Műegyetem rkp. 3., 1111 Budapest, Hungary; kramer.tamas@emk.bme.hu
* Correspondence: gadadhara.ferraz@emk.bme.hu

Abstract

River–aquifer exchange during floods controls groundwater recharge and bank storage, yet its sensitivity to floodplain geometry, flood duration, and subsurface permeability remains insufficiently quantified. A coupled model integrating one-dimensional surface-water flow, two-dimensional groundwater flow, and vertically resolved unsaturated floodplain infiltration was parameterized using observation-derived bank-storage estimates from Hungarian Danube floods. Idealized scenarios evaluated the effects of floodplain width, flood duration, and aquifer and soil permeability on river–aquifer exchange, bank storage, and flood attenuation. Simulations indicated that, under the investigated conditions, vertical floodplain infiltration dominates exchange processes, accounting for approximately 82–92% of total exchange and bank storage, whereas horizontal riverbed exchange remains secondary. Floodplain geometry and flood duration exerted influences on bank storage and flood attenuation comparable to those of subsurface permeability. Wider floodplains enhanced infiltration, storage capacity, and flood attenuation. Short floods produced high but transient infiltration and strong peak attenuation, whereas longer floods promoted sustained infiltration, larger bank storage, and delayed attenuation. Subsurface permeability regulated exchange efficiency but exhibited a nonlinear influence on bank storage. These results demonstrated that flood attenuation during overbank flooding depends not only on river–aquifer exchange magnitude, but also on its partitioning and the temporal evolution of subsurface storage.

Keywords: river–aquifer exchange; bank storage; flood attenuation; floodplain infiltration; overbank flooding; sensitivity analysis

Check for updates

Academic Editor: Salvatore Manfreda

Received: 4 June 2026
Revised: 14 July 2026
Accepted: 16 July 2026
Published: 18 July 2026

Copyright: © 2026 by the authors. Licensee MDPI, Basel, Switzerland. This article is an open access article distributed under the terms and conditions of the Creative Commons Attribution (CC BY) license.

1. Introduction

Flood hydrograph modification due to river–aquifer interactions is influenced by bank storage processes occurring through vertical floodplain infiltration and horizontal riverbed infiltration during rising river stages. Understanding these mechanisms is essential for accurately representing flood attenuation, groundwater recharge, and water balance dynamics in river–floodplain systems.

Early investigations into the role of bank storage focused primarily on in-bank flow processes and their influence on flood-wave propagation (e.g., [1–5]). While these studies established the importance of river–aquifer exchange, they generally neglected overbank flooding and floodplain inundation, which play a dominant role during large flood events. Recent developments in hydrological modeling have also highlighted the need to explicitly

represent floodplain connectivity and storage processes to realistically reproduce flood-wave routing and watershed hydrological response, particularly in floodplain-dominated river systems [6].

More recent studies have emphasized the importance of explicitly resolving floodplain inundation and infiltration processes [7–9]. In some systems, floodplain infiltration has been shown to dominate total exchange, contributing up to 88% of simulated infiltration during major floods [10], whereas in other cases its contribution remains limited, such as the Kuiseb River study [11], where floodplain infiltration increased total recharge by only 3%. These contrasting responses highlight the dependence of river–aquifer exchange on local hydraulic conditions, floodplain stratigraphy, and soil properties. Nevertheless, these studies focused primarily on water balance, residence time, ecological functioning, recharge estimation, or spatial patterns. Few investigations explicitly evaluated how vertical floodplain infiltration and horizontal riverbed exchange separately contribute to bank storage and how these pathways influence flood attenuation during overbank flooding.

In rivers with active floodplains, the floodplain topsoil is typically unsaturated prior to flood arrival, introducing an additional layer of complexity to river–aquifer exchange. Previous studies have shown that infiltration beneath inundated floodplains may be limited either by available unsaturated storage or by aquifer saturated hydraulic conductivity, depending on hydraulic conditions [7]. Variations in aquifer hydraulic conductivity can significantly alter infiltration fluxes and flood wave attenuation, with lower conductivities limiting subsurface flows and reducing hydrograph modification [1]. Similarly, clogging layers within the riverbed can attenuate groundwater responses and restrict river–aquifer connectivity [4], while flood processes, such as erosion, may modify hydraulic properties over time, affecting infiltration efficiency [12]. Previous sensitivity analyses have examined the influence of hydraulic properties and flood-wave characteristics on exchange fluxes and bank storage (e.g., [13]), but these studies largely focused on in-bank processes and neither explicitly considered infiltration across inundated floodplains nor evaluated how the relative contributions of vertical floodplain infiltration and horizontal riverbed exchange influence flood attenuation and storage dynamics during overbank flooding.

Numerical modeling has significantly advanced the understanding of river–aquifer interactions during flood events by enabling simulation of coupled surface water, groundwater, and floodplain infiltration processes under transient conditions. Early coupled approaches linked the Saint-Venant equations for channel flow with groundwater flow equations to demonstrate the role of bank storage in attenuating flood waves [1]. Subsequent developments led to the widespread application of groundwater-based models such as MODFLOW [14], including dedicated stream–aquifer interaction packages [15,16], as well as fully integrated surface–subsurface models such as MIKE SHE [17] and HydroGeoSphere [18], which simultaneously simulate surface flow, variably saturated flow, and groundwater flow. These physically based models explicitly simulate surface water, variably saturated flow, and groundwater, but their high computational demand and data requirements make them less suitable for systematic sensitivity analyses aimed at isolating the influence of geometry, flood duration, and hydraulic properties.

Despite these advances, many hydrodynamic models still neglect river–aquifer interactions or represent infiltration as a simplified loss term without groundwater feedback. Although several studies have attempted to address this limitation by coupling surface-water and groundwater models, many rely on restrictive assumptions. For example, some studies evaluated infiltration losses without explicitly representing groundwater feedbacks or dynamic bank-storage development [19], while others prescribed floodplain surface-water heads as fixed boundary conditions rather than deriving them from dynamically simulated overbank inundation [20]. Other studies focused on dryland or ephemeral river

systems [21]. Consequently, the applicability of these approaches to lowland alluvial rivers remains limited, where floodplain inundation, groundwater response, and bank-storage processes interact dynamically during overbank floods.

Relatively few studies have systematically evaluated how river–aquifer exchange and subsurface storage dynamics control flood attenuation during overbank flooding. For example, Hou et al. [19] examined infiltration effects through inundation extent, without explicitly distinguishing between vertical floodplain infiltration and horizontal riverbed exchange pathways.

This study addresses these gaps using a process-based coupled modeling framework that couples one-dimensional surface water flow, two-dimensional groundwater flow, and vertically unsaturated infiltration beneath the floodplain. The model is first parameterized and evaluated against observations from a representative Hungarian Danube reach and subsequently used as the benchmark configuration for one-at-a-time sensitivity analyses to investigate the influence of floodplain geometry, flood duration, and hydraulic properties on river–aquifer exchange, bank storage, and flood attenuation during overbank flooding. The objectives are to (1) quantify the relative contributions of vertical floodplain infiltration and horizontal riverbed exchange, (2) determine the relative importance of floodplain geometry, flood duration, and hydraulic properties in controlling bank storage, and (3) assess how these controls influence flood attenuation during overbank flooding.

2. Methodology

2.1. Overview of the Modeling Framework

The sensitivity analysis presented in this study uses a coupled numerical framework developed by the authors to simulate river–aquifer interactions during flood events. The complete model development, governing equations, numerical implementation, and verification are described by Ferraz and Krámer [22]. This section summarizes the methodological details required to understand and reproduce the sensitivity analyses, while the focus is placed on the physical interpretation of river–aquifer exchange processes and flood attenuation.

The framework integrates three components: (i) one-dimensional unsteady open-channel flow, (ii) two-dimensional groundwater flow, and (iii) vertically resolved infiltration beneath inundated floodplains. Surface water flow is simulated using the full Saint-Venant equations, where discharge and the water-surface elevation are solved simultaneously [23,24]. Groundwater flow is represented using a standard depth-integrated formulation based on Darcy's law and mass conservation [25], with the piezometric head as the state variable. Vertical infiltration is described using a Green–Ampt formulation to represent downward movement of the wetting front within initially unsaturated soils [26,27].

River–aquifer coupling is implemented through exchange fluxes between the surface-water and groundwater domains and explicitly separates two exchange pathways: horizontal riverbed infiltration and vertical floodplain infiltration (Figure 1).

The total river–aquifer specific flow rate is obtained by combining horizontal riverbed infiltration along the wetted channel perimeter with vertical infiltration integrated over the active floodplain width:

$$q_T = f_H P + \int_{2b_f} f_V \mathrm{d}y, \tag{1}$$

where q_T is the total exchange specific flow rate (dimension: $\mathrm{L}^2\ \mathrm{T}^{-1}$), P is the wetted perimeter associated with the main channel bed, excluding the floodplain sections (dimension: L), and $2b_f$ represents the active floodplain width (dimension: L).

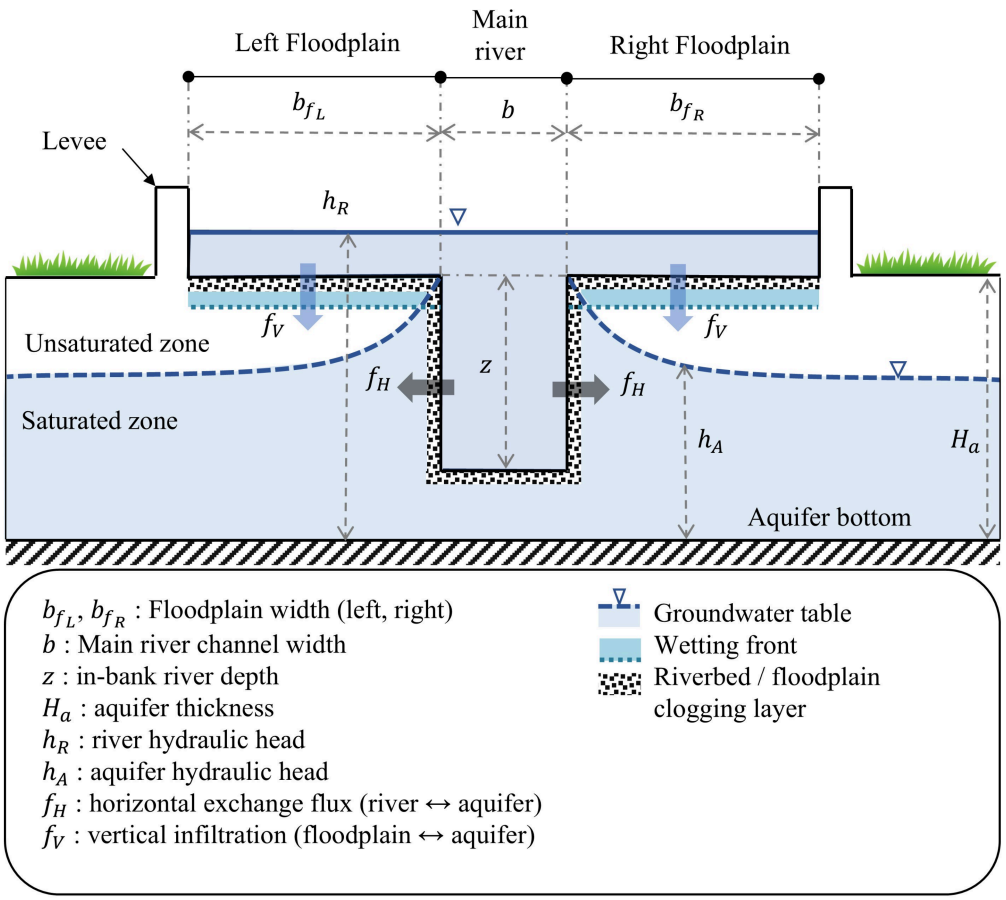


Figure 1. Conceptual representation of the coupled modeling framework. During overbank flooding, river–aquifer exchange occurs through two complementary pathways: (i) horizontal riverbed exchange (f_H) and (ii) vertical floodplain infiltration (f_V).

Horizontal exchange (f_H, dimension: L T^{-1}) occurs across the riverbed and is driven by hydraulic head differences between the river and aquifer. The exchange flux is calculated using Darcy's law:

$$f_H = \frac{K_{rb}}{m_{rb}}(h_R - h_A), \tag{2}$$

where K_{rb} is the hydraulic conductivity of the riverbed (dimension: L T^{-1}); m_{rb} is the riverbed layer thickness (dimension: L).

Vertical exchange (f_V, dimension: L T^{-1}) occurs only when river stages exceed bank elevation, activating infiltration through the unsaturated zone. Before saturation, vertical infiltration is computed using the Green–Ampt formulation, with infiltration controlled by soil hydraulic properties and local ponding depth, as follows:

$$f_V = K_z\left(1 + \frac{d - \psi_s}{W_F}\right), \tag{3}$$

where K_z is vertical hydraulic conductivity (dimension: L T^{-1}), d is water depth above the floodplain (dimension: L), ψ_s is soil suction head (dimension: L), and W_F is cumulative infiltration (dimension: L).

Once the wetting front reaches the groundwater table, the unsaturated Green–Ampt formulation is replaced by a saturated Darcy formulation:

$$f_V = \frac{K_z}{m}[h_R - \max(h_A, H_b)], \tag{4}$$

where m is the thickness of the interface layer beneath the floodplain (dimension: L).

The coupled model is implemented in MATLAB (Version 24.1, R2024a) using an explicit finite-difference scheme. Numerical stability is ensured through Courant-type restrictions, and exchange fluxes are imposed in a mass-conservative manner. Individual model components were previously verified against HEC-RAS, MODFLOW, and HYDRUS-1D [22].

We quantified river–aquifer exchange dynamics using the 50 km averaged specific flow rates from the river into the aquifer and the corresponding maximum specific bank storage volumes. Volumetric flow rates associated with vertical (Q_V) and horizontal (Q_H) infiltration were first computed at each model transect throughout the simulation period. For each transect, non-zero values of Q_V and Q_H were averaged over time and subsequently integrated along the 50 km model reach. Dividing by the reach length yielded the reach-averaged specific flow components q_V and q_H (i.e., per unit river length).

The resulting temporal evolution of specific bank storage was obtained by integrating Q_V and Q_H over the duration of the flood hydrograph. The maximum value of the resulting bank storage time series was then identified for each transect, integrated along the 50 km reach, and divided by the reach length to obtain the reach-averaged maximum specific bank storage components BS_V and BS_H. These values represent the total specific bank storage beneath the entire floodplain, including both the actively inundated and initially dry floodplain areas.

2.2. Idealized Geometry and Model Assumptions

To isolate the principal controls on river–aquifer exchange, the computational domain was idealized as a prismatic river reach with constant longitudinal slope. The river cross-section consists of a rectangular main channel bounded by symmetric floodplains. Small-scale topographic features, such as natural levees, depressions, or surface irregularities, are not represented. This assumption is appropriate for large leveed lowland rivers, such as the Hungarian reaches of the Danube and Tisza Rivers, where the active floodplain is inundated or dried within a small discharge interval. The results presented in this paper are therefore applicable primarily to rivers of this type.

In contrast, some rivers exhibit gradual and hysteretic floodplain inundation, weak lateral hydraulic connectivity, or persistent ponding after river stages recede. Valley morphology may further influence infiltration through transverse floodplain slopes [28] and localized depressions [20,29]. Representing such systems would require explicit small-scale topographic variability [30], which was intentionally excluded here to isolate first-order controls within a computationally efficient conceptual framework.

The aquifer is assumed to be homogeneous, isotropic, and temporally invariant. The aquifer extends well beyond the width of the active floodplain, so that it is practically unbounded laterally. Longitudinally, the computational domain extends well beyond the 50 km study reach, minimizing the influence of the downstream boundary condition.

These simplifications were adopted to isolate the influence of floodplain geometry, flood duration, and hydraulic properties on river–aquifer exchange, bank storage, and flood attenuation. Accordingly, the results should be interpreted as process-based sensitivities rather than site-specific predictions.

2.3. Model Parameterization and Validation

The benchmark model was parameterized using a representative 135 km reach of the Danube River between Dunaújváros and Mohács (rkm 1580–1446). Parameter selection was based on the 2013 flood event (approximately a 100-year recurrence interval).

The study reach is located within the Carpathian Basin, where Quaternary alluvial sediments consisting of alternating gravel, sand, silt, and clay layers form a heterogeneous unconfined aquifer system [31]. The alluvial aquifer is predominantly composed of coarse-grained sediments with relatively high horizontal hydraulic conductivity. Reported horizontal hydraulic conductivity values generally range from 10^{-4} to 8×10^{-3} m s^{-1} in gravelly deposits [32,33]. In contrast, vertical hydraulic conductivity is generally lower and more variable due to sediment layering and clogging processes, commonly ranging between 10^{-7} and 10^{-3} m s^{-1} [34]. Field studies further indicate substantial variability in floodplain sediments, with permeability influenced by sediment composition and clogging effects [35]. Effective porosity and specific yield are generally between 0.15 and 0.25 [36], providing substantial temporary groundwater storage during flood events. A representative specific yield of 0.21 was adopted for both the groundwater simulations and the estimation of observation-derived bank storage, ensuring consistency between the numerical model and the validation methodology.

Representative values of horizontal and vertical hydraulic conductivity were selected from literature-reported ranges for the Hungarian Danube following standard hydrogeological modeling practice [37]. Three coupled parameter sets representing low- ($K_x = 5$ md^{-1}, $K_z = 0.05$ md^{-1}), medium- ($K_x = 50$ md^{-1}, $K_z = 0.5$ md^{-1}), and high-connectivity ($K_x = 500$ md^{-1}, $K_z = 5$ md^{-1}) conditions were evaluated against observation-derived bank-storage estimates. Although these parameters describe different physical processes and are not necessarily correlated locally, they jointly control the hydraulic connectivity between the river and aquifer. They were therefore varied as coupled low-, medium-, and high-connectivity parameter sets to establish internally consistent benchmark parameterizations while limiting the number of calibration cases.

Preliminary simulations indicated that, under the investigated overbank flood conditions, variations in riverbed conductance had a considerably smaller effect on total bank storage than changes in floodplain geometry, flood duration, or aquifer hydraulic conductivity. Riverbed conductance was therefore held constant to isolate the principal controls investigated in this study while limiting the total number of benchmark scenarios.

Model parameterization targeted observation-derived estimates of bank storage beneath the dry floodplain (BS_{dry}), defined as the area extending approximately 3 km landward from the levees and representing the expected zone of flood-induced groundwater influence. A comparable approach for estimating bank storage from groundwater response was previously reported by Ubell [36]. Independent validation was subsequently performed using the 2002 and 2006 flood events.

Groundwater data were obtained from monitoring wells operated by the General Water Directorate of Hungary. Following quality control, stations containing substantial data gaps or inconsistent measurements were excluded. A total of 21 monitoring stations were retained for the 2013 parameterization event, while 14 and 18 stations were available for the 2002 and 2006 validation events, respectively. Because observations were available only beneath the dry floodplain, whereas measurements within the inundated floodplain and information on vadose-zone saturation were unavailable, total bank storage could not be estimated directly. Validation therefore focused on observation-derived bank storage beneath the dry floodplain (BS_{dry}), which integrates groundwater propagation resulting from both riverbed seepage and floodplain infiltration and thus provides an integrated indicator of flood-induced river–aquifer exchange intensity.

For each monitoring location, flood-induced groundwater rise was calculated as the difference between initial and peak groundwater heads. The resulting groundwater response was analyzed as a function of distance from the levee. Logarithmic attenuation curves were fitted to represent the spatial decay of groundwater response away from the

river, and the resulting profiles were integrated to estimate BS_{dry}. Storage estimates were subsequently scaled to a representative reach length of 50 km.

Initial groundwater conditions were derived from monitoring wells located within 900 m of the active floodplain, because this corresponds approximately to the average width of one side of the active floodplain along the analyzed reach. Mean groundwater heads were estimated as 87.99, 86.78, and 86.99 m a.s.l. for the 2013, 2002, and 2006 events, corresponding to unsaturated thicknesses of 2.43, 3.64, and 3.43 m, respectively.

Figure 2 shows the location of the benchmark Hungarian Danube reach together with the river gauge stations and groundwater observation wells used for model parameterization and validation.

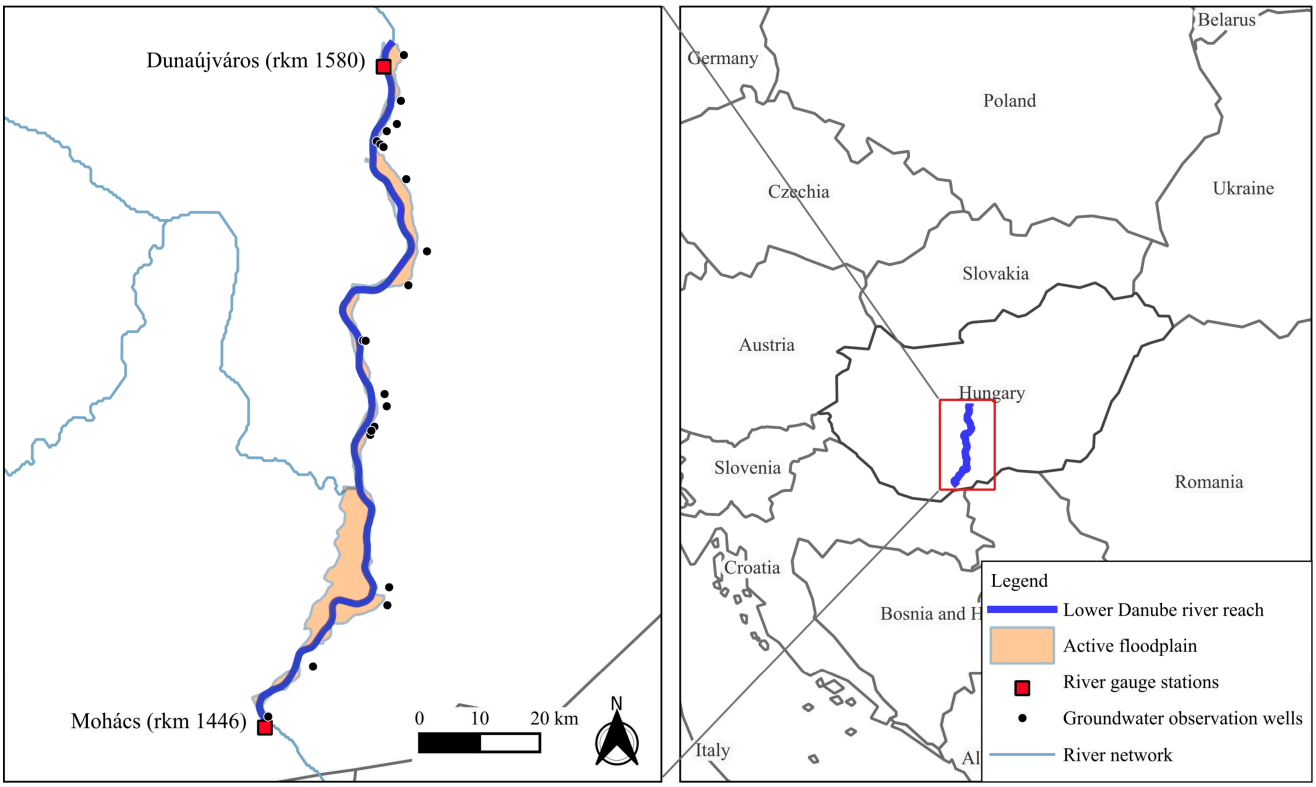


Figure 2. Location of 135 km long study reach of the Danube River in southern Hungary, the active floodplain, the river gauge stations at Dunaújváros (rkm 1580) and Mohács (rkm 1446), and the groundwater observation wells used for model parameterization.

Uncertainty in BS_{dry} estimation is partly associated with the identification of flood onset and antecedent groundwater conditions. Because storage estimates were derived from groundwater rise between initial and peak conditions, the selection of the initial state may influence the absolute storage volume. However, identical flood periods and initial conditions were used for both observation-derived estimates and numerical simulations, ensuring consistency during model evaluation.

Because validation is based on event-integrated estimates of bank storage rather than continuous groundwater-head time series, model performance was assessed using relative errors between simulated and observation-derived bank storage rather than conventional time-series performance metrics such as NSE or RMSE.

Although the benchmark model was parameterized for a representative Hungarian Danube reach, the objective of this study is to investigate the sensitivity of river–aquifer exchange processes rather than reproduce the behavior of a specific river system. Accordingly, the benchmark configuration was adopted as the reference case for the subsequent one-at-a-time sensitivity analyses. The reported findings should therefore be interpreted as

process-based insights applicable primarily to large alluvial river–floodplain systems with comparable hydrogeological characteristics.

Model evaluation is based on one calibration event and two independent validation events, reflecting the limited availability of simultaneous flood and groundwater observations for large overbank floods. Although these events provide encouraging support for the adopted modeling framework, additional validation using a larger number of flood events and direct observations beneath inundated floodplains would further increase confidence in the estimated exchange partitioning.

2.4. Sensitivity Analysis Design

The sensitivity analysis considers three groups of scenarios representing the principal physical controls on river–aquifer exchange during overbank flooding: (i) floodplain geometry, (ii) overbank flood duration, and (iii) aquifer and soil hydraulic properties. Each scenario group isolates one controlling factor while maintaining all remaining parameters at their reference values.

Floodplain geometry is parameterized using the ratio of total floodplain width to main channel width (B_f/b), which controls the available inundation area and the potential storage volume for floodplain infiltration. Values of B_f/b = 3, 5, and 9 represent progressively wider floodplains ranging from moderately confined river corridors to extensive alluvial systems. These values are broadly representative of lowland rivers such as the two major rivers of Hungary, the Danube and the Tisza.

In the present study, overbank flood duration is used as a surrogate descriptor of flood hydrograph duration while preserving the overall flood shape. The reference configuration was derived from the 2013 flood on the Hungarian Danube. Sensitivity to flood duration was evaluated by varying the overbank inundation period ($T_{overbank}$), controlling the time available for river–aquifer exchange. In addition to a reference flood event, shorter- and longer-duration scenarios were generated by scaling the overbank flooding duration to $T_{overbank}/2$ and $2T_{overbank}$, respectively. These variations represent generalized hydrograph types, with shorter durations corresponding to flashy flood events and longer durations representing more sustained flooding conditions commonly observed in lowland river systems.

The inflow hydrographs used in the simulations are shown in Figure 3. Simulations are terminated at the end of the respective inflow hydrograph, i.e., at day 15, 30, or 60.

Aquifer and soil hydraulic properties determine the capacity of the subsurface to transmit and store water. Hydraulic parameter sets corresponding to sand (High K), sandy loam (Medium K), and clay loam (Low K) soil types were adopted using literature-derived values representative of typical river–floodplain systems (Section 2.3). Although natural soils exhibit spatial variability, these values are used to capture representative hydraulic behavior and enable systematic comparison of contrasting permeability conditions.

While the model setup is idealized, these parameter ranges are consistent with those observed in real river–aquifer systems and are intended to capture the dominant controls on infiltration and bank storage processes under overbank flooding conditions.

Sensitivity analyses are conducted by varying one parameter group at a time—floodplain geometry (S1), flood duration (S2), and subsurface hydraulic properties (S3)—while all remaining parameters are kept at their reference values. Hydraulic properties in S3 were varied collectively to preserve physically realistic soil parameter combinations. This one-at-a-time design isolates the first-order influence of each parameter group and facilitates physical interpretation of the governing mechanisms. Consequently, the reported sensitivities represent isolated effects relative to the benchmark configuration rather than a complete quantification of parameter interactions.

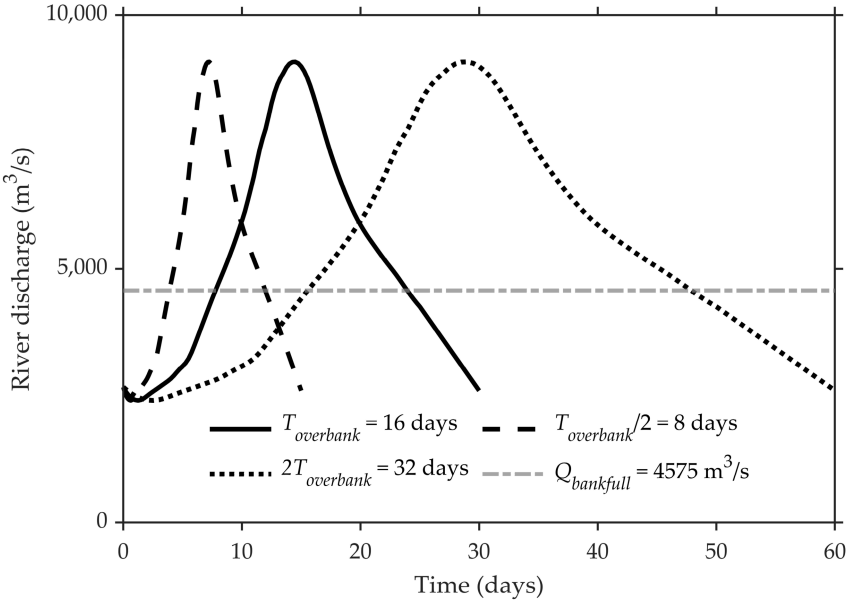


Figure 3. Inflow hydrographs, considering short overbank flood duration ($T_{overbank}/2 = 8$ d), and long overbank flood duration ($2T_{overbank} = 32$ d), and the baseline scenario ($T_{overbank} = 16$ d). Bankfull discharge ($Q_{bankfull} = 4575$ m^{3}s^{-1}) is also shown.

Table 1 lists the principal river and subsurface hydraulic parameters defining this idealized river–aquifer system.

Table 1. Reference hydraulic and geometric parameters adopted in the benchmark model together with the parameter values used in the three sensitivity analyses. Parameters not included within a sensitivity group remain unchanged at their reference values.

Parameter	Parameter Values			Unit	Description
	Low	Reference	High		
b		475		m	Width of the main channel
z		9.00		m	Depth of the main channel
S_0		7×10^{-5}		m m^{-1}	Longitudinal bed slope
n_m		0.033		s m$^{-1/3}$	Manning roughness of the main channel
n_f		0.1		s m$^{-1/3}$	Manning roughness of the floodplain
K_{rb}/m_{rb}		0.15		d^{-1}	Riverbed leakage = riverbed hydraulic conductivity/thickness of the interface layer
S_y		0.21		-	Specific yield for unconfined aquifer conditions
S_s		1×10^{-5}		m^{-1}	Specific storage
H_a		24.00		m	Aquifer thickness
h_{A0}		21.57		m	Initial hydraulic head in the aquifer
			S1—floodplain geometry		
B_f/b	3	5	9	-	Floodplain width ratio
b_f	450	900	1800	m	Width of one side of the floodplain
B_f	1375	2275	4075	m	Total overbank width ($B_f = 2b_f + b$)
$h_R(max)$	27.61	27.00	26.29	m	Maximum height of the river water surface above the aquifer bottom for the geometry scenarios

Table 1. *Cont.*

Parameter	Parameter Values			Unit	Description
	Low	Reference	High		
			S2—flood duration		
$T_{overbank}$	8	16	32	d	Overbank flooding duration
$h_R(max)$	26.60	27.00	27.27	m	Maximum height of the river water surface above the aquifer bottom for the overbank flood duration scenarios
			S3—hydraulic properties		
Soil Type	Clay Loam	Sandy Loam	Sand	-	
$K_a = K_x$	5	50	500	m d^{-1}	Aquifer horizontal hydraulic conductivity
θ_r	0.08	0.04	0.02	cm^3 cm^{-3}	Residual water content
θ_s	0.46	0.45	0.44	cm^3 cm^{-3}	Saturated water content
ψ_s	0.56	0.30	0.16	m	Capillary suction head at the wetting front
K_z	0.05	0.5	5	m d^{-1}	Saturated vertical hydraulic conductivity

Sensitivity was evaluated using changes in key hydrodynamic indicators relative to the benchmark configuration, including vertical and horizontal exchange fluxes, bank storage, peak discharge attenuation, surface-water level, and peak timing. A normalized relative sensitivity index (S_r) was evaluated following the concept of dimensionless sensitivity coefficients [38]:

$$S_r^- = \frac{(Y_{low} - Y_0)/Y_0}{(X_{low} - X_0)/X_0}, \quad (5)$$

$$S_r^+ = \frac{\left(Y_{high} - Y_0\right)/Y_0}{\left(X_{high} - X_0\right)/X_0}, \quad (6)$$

where X_0 and Y_0 denote the parameter value and corresponding response for the reference scenario, while X_{low}, Y_{low}, X_{high}, and Y_{high} represent the lower and higher parameter scenarios, respectively.

The temporal evolution of exchange fluxes and bank storage was additionally studied to characterize process dynamics.

2.5. Dimensionless Recharge Indicator $\boldsymbol{F^*}$ *and Infiltration Pathway Indicator* $\boldsymbol{P^*}$

To facilitate interpretation of the sensitivity analyses, two additional dimensionless indicators were evaluated. The pathway indicator (P^*) quantifies the relative contribution of vertical floodplain infiltration and horizontal riverbed exchange to bank storage during overbank flooding, whereas the recharge indicator (F^*) characterizes the dominant physical limitation on river–aquifer recharge.

P^* was calculated as

$$P^* = BS_V^+ / BS_H^+, \quad (7)$$

where (BS_V^+) and (BS_H^+) represent the cumulative positive bank-storage contributions associated with vertical floodplain and horizontal riverbed exchange, respectively. P^* is defined only for overbank flood conditions. Values of $P^* > 1$ indicate that vertical floodplain infiltration contributes more to bank storage than horizontal riverbed exchange, whereas values of $0 < P^* < 1$ indicate dominance of horizontal riverbed exchange. In the absence of overbank flooding, $BS_V = 0$ and therefore $P^* = 0$.

To interpret the simulated recharge processes within an established conceptual framework, the dimensionless recharge indicator (F^*) proposed by Doble et al. [39] was also evaluated. Following the original formulation, F^* compares the maximum potential infiltration with the combined capacity of the aquifer to store and laterally transmit infiltrated water. For the present model, the indicator was adapted by (i) including both vertical floodplain infiltration and horizontal riverbed exchange in the potential infiltration term (I), and (ii) replacing the lateral outflow term (Q) beyond the active floodplain with the analytical solution of a step-function driven Darcy flow into a confined aquifer:

$$F^* = \frac{I}{\Delta S + Q} = \frac{\frac{K_z}{m}\left(2b_f\right)[h_R(max) - H_a]T_{overbank} + \frac{K_{rb}}{m_{rb}}P[h_R(max) - h_{A0}]T_{flood}}{(H_a - h_{A0})b_f S_y + 2(H_a - h_{A0})\sqrt{\frac{K_a H_a S_y T_{overbank}}{\pi}}}, \quad (8)$$

where m is the equivalent thickness of the floodplain clogging layer calibrated to reproduce the Green–Ampt infiltration response, T_{flood} is the flood duration above the initial water level, and the remaining variables are defined in Sections 2.1–2.4 and Table 1.

Following Doble et al. [39], values of $F^* > 1$ indicate that recharge is primarily limited by the resistance of the clogging layer, whereas values of $F^* < 1$ indicate limitation by unsaturated aquifer storage capacity and horizontal transmissivity.

3. Results

3.1. Model Parameterization and Validation Results

The benchmark model was evaluated by comparing simulated and observation-derived estimates of bank storage beneath the dry floodplain (BS_{dry}) for one parameterization event (2013) and two independent validation events (2006 and 2002). Observation-derived storage estimates were derived from groundwater monitoring data using the procedure described in Section 2.3. Although this dataset is limited by the availability of suitable field observations during large overbank floods, it provides an independent assessment of the model's ability to reproduce flood-induced groundwater responses beneath the dry floodplain.

Figure 4 shows the observed groundwater response as a function of distance from the levee for the three analyzed flood events, together with the logarithmic attenuation curves used to estimate BS_{dry}. Groundwater response decreased systematically with increasing distance from the levee for all three events, supporting the use of logarithmic attenuation functions to estimate observation-derived BS_{dry}.

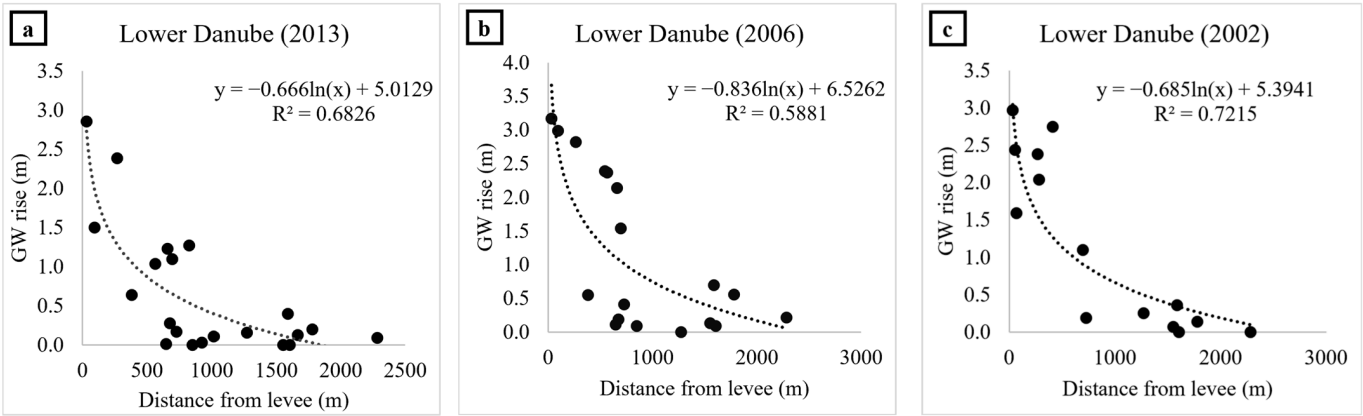


Figure 4. Maximum observed groundwater rise as a function of distance from the levee for the Hungarian Danube during the (**a**) 2013, (**b**) 2006 and (**c**) 2002 flood events. Dotted curves indicate logarithmic regressions used to estimate BS_{dry}.

Observation-derived estimates of BS_{dry} ranged from 25 to 43 $\times$ 10^6 m^3 (Table 2), corresponding to normalized values (BS_{dry}/L_x) ranging from 2.50 $\times$ 10^5 to 4.30 $\times$ 10^5 m^3 km^{-1} per river side. These values compare well with the estimate reported by Ubell [36] for the 1958 Danube flood in the Szigetköz region (2.31 $\times$ 10^5 m^3 km^{-1}) which was derived for the Hungarian side of the Danube. The remaining differences likely reflect variations in flood magnitude, local hydrogeological conditions, and the spatial extent of groundwater response.

Table 2. Simulated and observation-derived ("Measured") bank storage beneath the dry floodplain (BS_{dry}, 10^6 m^3) for the Hungarian Danube parameterization and validation events.

Conductivity Scenario	2013 Flood			2006 Flood			2002 Flood		
	Numerical Model	Measured	Relative Error (%)	Numerical Model	Measured	Relative Error (%)	Numerical Model	Measured	Relative Error (%)
SCN25 (low K)	3	25	−87%	5	43	−88%	0	37	−100%
SCN26 (medium K)	24	25	−5%	33	43	−23%	26	37	−31%
SCN27 (high K)	80	25	218%	110	43	157%	90	37	142%

Simulated BS_{dry} values varied by more than one order of magnitude across the three hydraulic conductivity scenarios, confirming strong dependence of bank storage on aquifer hydraulic properties. Among the tested scenarios, the medium-conductivity configuration provided the best agreement with observations, reproducing the parameterization event (2013) within approximately 5% and the two independent validation events (2006 and 2002) within 23–31% (Table 2).

The agreement obtained for the three analyzed flood events supports the suitability of the medium-conductivity scenario as the benchmark configuration for the subsequent sensitivity analyses. Accordingly, the medium-conductivity scenario was adopted as the benchmark configuration, while the low- and high-conductivity scenarios were retained as representative end-member conditions for evaluating the influence of hydraulic properties. Nevertheless, the validation dataset remains limited, and additional flood events and direct measurements beneath inundated floodplains would be valuable for further assessing the robustness of the simulated exchange partitioning.

3.2. Integrated River–Aquifer Exchange Response

River–aquifer exchange was quantified using reach-averaged vertical and horizontal specific flow rates (q_V and q_H) and the corresponding maximum specific bank storage components (BS_V and BS_H). Mean exchange fluxes were averaged over the simulation period, whereas bank storage corresponds to the maximum cumulative storage developed during each simulation. All quantities are reported per unit river length and summarized in Table 3.

Across all scenarios, vertical floodplain infiltration is the dominant exchange pathway. The simulated mean vertical specific flow rate (q_V) accounts for approximately 82–92% of the simulated total specific flow rate (q_T), whereas horizontal riverbed exchange (q_H) contributes only 8–18%. A similar partitioning is observed for bank storage, where BS_V consistently exceeds BS_H. Because direct observations beneath inundated floodplains are unavailable, these percentages should be interpreted as model-derived estimates for the investigated conditions rather than directly validated field values.

The magnitude of river–aquifer exchange varies substantially among the three sensitivity groups. Increasing floodplain width from $B_f/b = 3$ to 9 increases maximum specific bank storage by approximately 140%, whereas extending overbank flood duration from 8 to 32 days increases bank storage by about 31%. Increasing hydraulic conductivity from Clay Loam to Sand increases maximum bank storage by approximately 150%. These results

demonstrate that floodplain geometry exerts control on bank storage comparable to, or greater than, that of subsurface hydraulic properties.

Table 3. Mean vertical and horizontal components of specific infiltration flow from the river into the aquifer, and their total (q_V, q_H, q_T), averaged over the simulation period. The associated maximum specific bank storage volumes (BS_V, BS_H, BS_T), for all scenarios. All variables are averaged/integrated over the 50 km river length.

Scenario Group	Scenario	Mean q_V	Mean q_H	Mean q_T	Max BS_V	Max BS_H	Max BS_T
		[$m^3\ s^{-1}\ km^{-1}$]	[$m^3\ s^{-1}\ km^{-1}$]	[$m^3\ s^{-1}\ km^{-1}$]	[$10^6\ m^3\ km^{-1}$]	[$10^6\ m^3\ km^{-1}$]	[$10^6\ m^3\ km^{-1}$]
S1—floodplain geometry	$B_f/b = 3$	0.56	0.12	0.68	0.85	0.12	0.97
		82%	18%		88%	12%	
	$B_f/b = 5$	0.82	0.12	0.94	1.31	0.12	1.43
		87%	13%		92%	8%	
	$B_f/b = 9$	1.31	0.12	1.43	2.22	0.13	2.35
		92%	8%		94%	6%	
S2—flood duration	$T_{overbank}/2$	1.39	0.17	1.56	1.17	0.09	1.26
		89%	11%		93%	7%	
	$T_{overbank}$	0.82	0.12	0.94	1.31	0.12	1.43
		87%	13%		92%	8%	
	$2T_{overbank}$	0.49	0.08	0.57	1.49	0.17	1.65
		86%	14%		90%	10%	
S3—soil and aquifer type	Clay Loam	0.56	0.09	0.65	0.91	0.11	1.02
		86%	14%		90%	10%	
	Sandy Loam	0.82	0.12	0.94	1.31	0.12	1.43
		87%	13%		92%	8%	
	Sand	1.50	0.23	1.73	2.35	0.23	2.57
		87%	13%		91%	9%	

3.3. Sensitivity to Floodplain Geometry (S1)

Floodplain geometry exerts a strong control on river–aquifer exchange processes by regulating the extent of inundated area available for vertical infiltration. Increasing the floodplain-to-channel width ratio (B_f/b) from 3 to 9 results in a greater total river-to-aquifer exchange, driven by enhanced vertical infiltration from the floodplain.

Mean vertical specific flow rates increase from 0.56 $m^3\ s^{-1}\ km^{-1}$ for $B_f/b = 3$ to 1.31 $m^3\ s^{-1}\ km^{-1}$ for $B_f/b = 9$ (Table 3), corresponding to an increase of more than 130%. In contrast, mean horizontal specific flow rates through the riverbed remain nearly constant across all floodplain configurations, with values close to 0.12 $m^3\ s^{-1}\ km^{-1}$. As a consequence, the contribution of vertical to the mean total specific flow rate increases with floodplain width, accounting for approximately 82% of total infiltration for $B_f/b = 3$ and exceeding 90% for the widest floodplain configuration.

Total specific bank storage rises from 0.97×10^6 $m^3\ km^{-1}$ for $B_f/b = 3$ to 2.35×10^6 $m^3\ km^{-1}$ for $B_f/b = 9$ (Table 3). The increase is almost entirely associated with vertical bank storage (BS_V), whereas bank storage produced by horizontal exchange (BS_H) remains nearly constant across all scenarios. For all floodplain configurations, the simulations indicate that more than 88% of total bank storage originates from vertical infiltration, reaching up to 94% for the widest floodplain.

However, the increase in floodplain width does not produce a proportional increase in mean specific flow and bank storage. This sublinear response likely reflects the combined effect of increased infiltration area and reduced ponding depth over wider floodplains. While a larger floodplain provides more area for vertical infiltration, the same flood hy-

drograph is distributed over a wider inundated surface, reducing the local head above the floodplain soil and thereby limiting the increase in vertical infiltration flux. In contrast, horizontal exchange is driven primarily by the hydraulic gradient between the river and aquifer near the channel, which explains its weak sensitivity to floodplain width. This distinction further highlights the importance of explicitly separating vertical and horizontal exchange pathways in the model.

The influence of floodplain geometry on river–aquifer exchange is illustrated in Figure 5 by the temporal evolution of horizontal and vertical infiltration volumetric flow rates, Q_H and Q_V, integrated over the 50 km river reach, and the associated bank storage components for increasing floodplain width ratios (B_f/b = 3, 5, and 9).

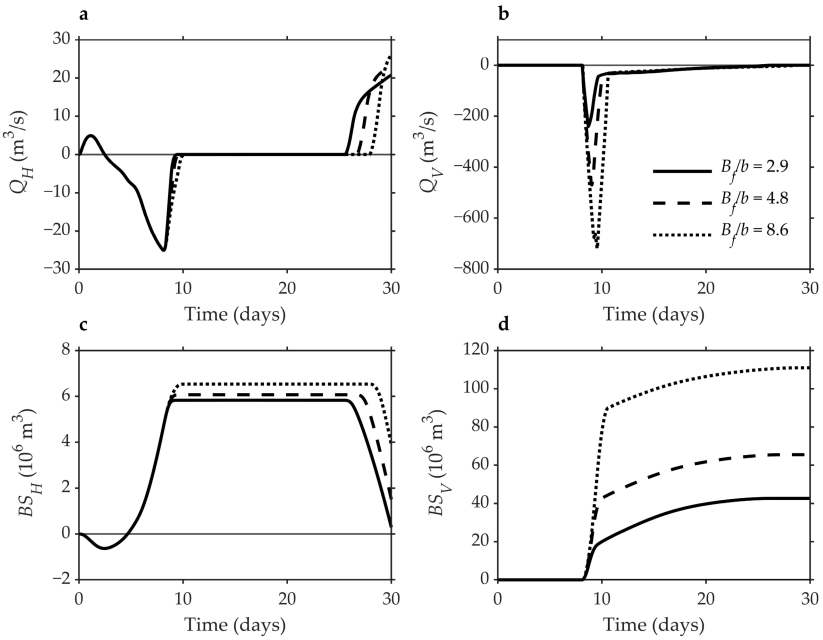


Figure 5. Temporal evolution of infiltration volumetric flow rates and associated bank storage components for the floodplain geometry sensitivity analysis (S1). (**a**) Horizontal volumetric flow rate (Q_H) for all floodplain width ratios (B_f/b = 3, 5, and 9). (**b**) Vertical volumetric flow rate (Q_V). (**c**) Bank storage associated with Q_H (BS_H). (**d**) Bank storage associated with Q_V (BS_V).

The evolution of Q_H (Figure 5a) shows a similar temporal pattern across all floodplain configurations. During the rising limb, Q_H initially flows from the aquifer toward the river before reversing as river stages rise. Peak magnitude and timing are nearly identical for all floodplain widths, indicating that riverbed exchange is governed primarily by river-stage dynamics rather than floodplain geometry.

In contrast, the evolution of Q_V (Figure 5b) exhibits dependence on floodplain width (once overbank inundation occurs). Following overbank inundation, Q_V increases sharply in all scenarios, with both peak magnitude and duration increasing with floodplain width. Wider floodplains maintain larger infiltration rates throughout the inundation period despite the gradual reduction in hydraulic gradients caused by increasing groundwater storage.

These contrasting flow rate dynamics are reflected in the evolution of bank storage components. BS_H (Figure 5c) follows a similar trajectory in all scenarios, reaching a plateau, reflecting the limited contribution of horizontal infiltration, which diminishes as hydraulic gradients in the near-river zone decrease, and exhibiting only modest sensitivity to floodplain width. In contrast, BS_V (Figure 5d) increases sharply following floodplain inundation and shows a pronounced dependence on floodplain extent. Wider floodplains

lead to both faster accumulation and larger volumes of vertical bank storage, with storage continuing to increase throughout the inundation period.

3.4. Sensitivity to Overbank Flood Duration (S2)

Overbank flood duration exerts a control on the temporal characteristics of river–aquifer exchange, producing contrasting effects on specific infiltration flow rates and specific bank storage. Variations in flood duration primarily modify the time available for infiltration and groundwater redistribution, thereby governing the balance between exchange intensity and cumulative storage accumulation.

Short-duration flood events ($T_{overbank}/2$) produce the highest mean total specific flow rates (1.56 $m^3\ s^{-1}\ km^{-1}$), but the smallest maximum specific bank storage ($1.26 \times 10^6\ m^3\ km^{-1}$). In contrast, extending flood duration to $2T_{overbank}$ sustains infiltration for longer periods, increasing maximum bank storage to $1.65 \times 10^6\ m^3\ km^{-1}$ despite reducing the mean specific infiltration rate to 0.57 $m^3\ s^{-1}\ km^{-1}$.

Across all flood-duration scenarios, the simulations indicate that vertical infiltration remains the dominant exchange mechanism, consistently contributing approximately 90% of total bank storage. Horizontal infiltration through the riverbed exhibits only minor sensitivity to flood duration.

Figure 6 illustrates the temporal evolution of the vertical and horizontal components and their cumulative contribution to bank storage under different overbank flooding durations. The results highlight a trade-off between infiltration intensity and duration, where short floods generate rapid exchange pulses and long floods sustain infiltration over extended periods.

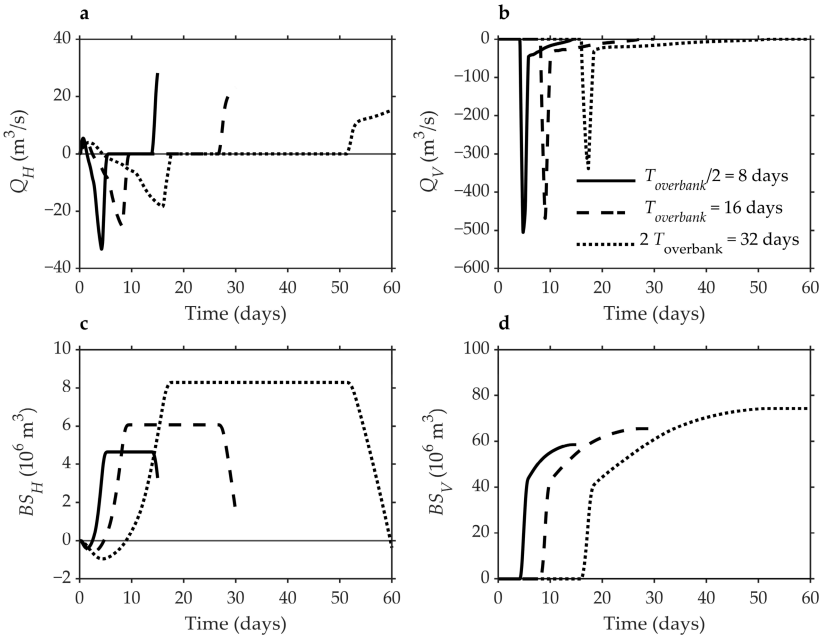


Figure 6. Temporal evolution of infiltration volumetric flow rates and associated bank storage components for the overbank flood duration sensitivity analysis (S2). (**a**) Horizontal volumetric flow rate (Q_H) for all overbank flood durations ($T_{overbank}/2$, $T_{overbank}$, $2T_{overbank}$). Descriptions of (**b**–**d**) are presented in Figure 5.

Short-duration flooding induces a horizontal volumetric flow rate (Q_H) peak shortly after the onset of river flow, driven by steep and rapidly evolving hydraulic gradients between the river and the aquifer. As flood duration increases, these peak values diminish, while Q_H persists over longer periods, reflecting a more gradual equalization of groundwater heads. Horizontal bank storage (BS_H; Figure 6c) increases rapidly during the early

stages of flooding and reaches a plateau shortly after peak Q_H occurs, driven by the gradual reduction in Q_H.

Vertical volumetric flow rates (Q_V) dominate total river–aquifer exchange and exhibit a pronounced sensitivity to flood duration (Figure 6b). The shortest overbank event generates the highest instantaneous infiltration fluxes, associated with large ponding depths over initially unsaturated floodplain soils; however, these high flows are short-lived, reflecting the shorter flood duration. In contrast, longer-duration floods produce lower peak Q_V values but sustain infiltration over extended periods.

This shift from intensity-driven to duration-controlled infiltration governs the cumulative storage response. Vertical bank storage (BS_V; Figure 6d) exhibits a different behavior. Short-duration floods lead to rapid storage accumulation but reach comparatively low maximum volumes due to the limited infiltration window. As flood duration increases, vertical flows allow continued accumulation over time, resulting in larger maximum storage volumes despite lower instantaneous infiltration fluxes. This explains the apparent contrast observed in Table 3, where shorter floods yield higher mean specific flow rates, whereas longer-duration events produce the greatest total and maximum bank storage.

3.5. Sensitivity to Soil and Aquifer Hydraulic Properties (S3)

The hydraulic properties of the aquifer and the unsaturated soil control both horizontal and vertical infiltration and, consequently, the development of bank storage. The hydraulic parameters were varied collectively to represent three characteristic soil types (Clay Loam, Sandy Loam, and Sand), preserving physically consistent combinations of saturated and unsaturated hydraulic properties.

Mean total specific infiltration flows increase markedly from 0.65 $m^3\ s^{-1}\ km^{-1}$ for the Clay Loam scenario to 1.73 $m^3\ s^{-1}\ km^{-1}$ for the Sand scenario. This increase is primarily driven by a rise in mean vertical specific flow rate (q_V), which nearly triples across the considered soil types. In contrast, mean horizontal specific flow rate (q_H) exhibits a more moderate increase and remains secondary to q_V in all scenarios. Consequently, q_V consistently accounts for more than 86% of the total river–aquifer exchange, confirming its dominant role irrespective of soil type.

The influence of subsurface hydraulic properties is even more pronounced in the development of bank storage. Maximum total bank storage volumes increase from $1.02 \times 10^6\ m^3\ km^{-1}$ for the clay loam scenario to $2.57 \times 10^6\ m^3\ km^{-1}$ for the sand scenario, corresponding to an increase of more than 150%. The increase is driven almost entirely by vertical bank storage, whereas the contribution of horizontal storage remains close to 10% across all soil types.

However, the response is nonlinear. Although hydraulic conductivity increases by approximately two orders of magnitude between the analyzed soil types, infiltration rates increase by only about a factor of three. This indicates that river–aquifer exchange is not controlled solely by permeability. As hydraulic conductivity increases, recharge becomes increasingly constrained by available water volume, aquifer storage capacity, and groundwater redistribution.

Figure 7 shows the temporal evolution of horizontal and vertical infiltration and the associated bank storage for the three soil types.

Q_H remains consistently smaller in magnitude than Q_V (Figure 7a). More permeable soils, such as Sand, induce higher and more gradually developed Q_H peaks compared to finer-textured soils.

Q_V exhibits a sensitivity to soil and aquifer hydraulic properties (Figure 7b), particularly when comparing Clay Loam and Sand scenarios. Clay Loam produces nearly constant infiltration throughout the flood because low hydraulic conductivity limits in-

filtration even under favorable hydraulic gradients. In contrast, Sandy Loam and Sand generate pronounced Q_V peaks prior to soil saturation, followed by sustained infiltration over extended periods once saturated conditions are reached, as hydraulic gradients progressively decrease.

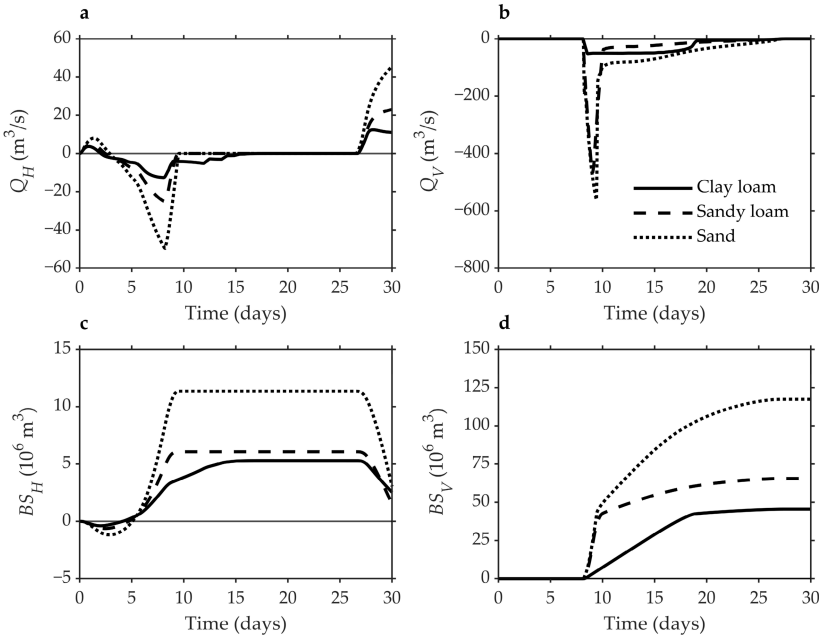


Figure 7. Temporal evolution of infiltration volumetric flow rates and associated bank storage components for the soil and aquifer hydraulic property sensitivity analysis (S3). (**a**) Horizontal volumetric flow rate (Q_H) for all soil types (Clay Loam, Sandy Loam, Sand). Descriptions of (**b**–**d**) are presented in Figure 5.

Consistent with the flow behavior, both BS_H (Figure 7c) and BS_V (Figure 7d) increase more rapidly under higher-permeability conditions, with vertical storage dominating total bank storage across all scenarios.

In the low-permeability Clay Loam scenario, BS_V development is primarily constrained by limited soil hydraulic conductivity, which restricts infiltration even under favorable hydraulic gradients. In contrast, for the more permeable Sandy Loam and Sand scenarios, infiltration responds rapidly to inundation, and storage development becomes increasingly controlled by the temporal characteristics of the flood hydrograph, particularly the duration and steepness of the rising limb.

3.6. Regime Analysis Using the Dimensionless Recharge Indicator $\boldsymbol{F}^*$ *and Infiltration Pathway Indicator* $\boldsymbol{P}^*$

The pathway indicator P^*, defined in Section 2.5, ranges from 7.3 to 17.0, showing that vertical infiltration contributes substantially more to bank storage than horizontal riverbed infiltration under the investigated overbank flood conditions. Floodplain geometry produces the strongest variation in P^*, with wider floodplains increasing vertical dominance through expansion of the inundated area. In contrast, flood duration and hydraulic properties produce smaller changes in P^*, indicating that these parameters mainly affect bank storage magnitude rather than the relative contribution of vertical and horizontal pathways.

All scenarios yielded values substantially greater than unity ($F^* = 24$–647), indicating that the investigated system remains within a clogging-layer-controlled recharge regime throughout the examined parameter space and across the range of river and floodplain conditions considered in this study. Thus, recharge is controlled primarily by the hydraulic

resistance of the floodplain and riverbed interface layers rather than by aquifer storage capacity or horizontal transmissivity.

Although the magnitude of F^* varies between scenarios, all cases remain within the same recharge regime. Consequently, the observed differences in simulated bank storage arise from variations in floodplain geometry, flood duration, and hydraulic properties rather than from a transition between recharge regimes.

3.7. Implications for Flood Attenuation

The sensitivity analyses suggest that river–aquifer exchange processes exert a moderate control on flood wave transformation, infiltration timing, and transient water storage within the floodplain–aquifer system through the combined effects of floodplain geometry, flood duration, and subsurface hydraulic properties (Table 4).

Table 4. Summary of flood peak attenuation and flood-wave timing effects induced by river–aquifer exchange across all sensitivity scenarios. The columns "With exchange" correspond to simulations in which both horizontal riverbed exchange and vertical floodplain infiltration are represented, whereas "No exchange" corresponds to simulations with an impermeable riverbed–floodplain interface, preventing any exchange between the river and the aquifer. Reported values represent relative reductions in peak discharge ($\Delta Q_{peak}/Q_{peak}$) and reductions in peak water level (Δh_{peak}), compared to simulations without river–aquifer exchange.

Scenario Group	Scenario	$\Delta Q_{peak}/Q_{peak}$ (With Exchange, %)	$\Delta Q_{peak}/Q_{peak}$ (No Exchange, %)	Δh_{peak} (With Exchange, cm)	Δh_{peak} (No Exchange, cm)
S1	$B_f/b = 3$	2.2%	1.9%	14.48	12.17
	$B_f/b = 5$	3.8%	3.4%	20.67	17.58
	$B_f/b = 9$	6.2%	5.6%	26.63	22.01
S2	$T_{overbank}/2$	7.8%	7.1%	37.71	32.54
	$T_{overbank}$	3.8%	3.4%	20.67	17.58
	$2T_{overbank}$	1.5%	1.3%	8.95	7.32
S3	Clay Loam	3.9%	3.4%	20.80	17.58
	Sandy Loam	3.8%	3.4%	20.67	17.58
	Sand	4.3%	3.4%	23.59	17.58

Across all scenario groups, infiltration reduces peak river discharge with distance and delays its timing relative to the no-infiltration cases. However, the attenuation mechanism differs between scenarios.

In S1 (floodplain geometry), increasing floodplain width enhanced both infiltration and bank-storage development through expansion of the inundated area and increased vertical exchange. Peak discharge attenuation increased from approximately 2% to 6%, while peak timing delays increased by up to 9 h. Relative sensitivity coefficients ($S_r^- = 1.03$, $S_r^+ = 0.82$) indicated that attenuation responds almost proportionally to floodplain width. The slightly larger sensitivity associated with floodplain reduction suggests that attenuation is more strongly affected by loss of floodplain storage capacity than by equivalent floodplain expansion.

Flood duration (S2) governs the balance between infiltration intensity and cumulative storage. Short-duration floods exhibit the largest reductions in river flow (7.8%) and water level (37.71 cm) due to steep hydraulic gradients and high vertical exchange. However, their limited duration restricts the development of bank storage, resulting in smaller delays in peak outflow timing ($\Delta t = 11$ h). In contrast, prolonged floods produce lower flow attenuation (1.5%) but increase bank storage, leading to longer peak delays ($\Delta t = 14$ h). Relative sensitivity analysis showed asymmetric behavior, with strong positive sensitivity for reduced flood duration ($S_r^- = 1.03$) and negative sensitivity for increased duration ($S_r^+ = -0.60$). These results suggest that flood attenuation can be governed either by

short-lived peak reduction during brief floods or by sustained subsurface storage during longer floods, depending primarily on flood duration and shape rather than peak water level alone. An advantage of the vertical infiltration pathway is that it is activated only in the overbank phase, so it preserves more of the aquifer's storage capacity for maximal peak reduction. In contrast, the horizontal infiltration pathway may saturate the aquifer prematurely, reducing its effectiveness during the actual peak.

Subsurface hydraulic properties (S3) influence flow attenuation while exerting a limited effect on flood-wave timing. High-conductivity soils (sand) lead to greater reductions in both peak discharge (4.3%) and peak water levels (23.59 cm) compared to lower-conductivity conditions. In contrast, differences in peak timing between soil types are minor, with only slight delays in peak stage observed (on the order of a few hours), and negligible changes in peak discharge timing. Relative sensitivity values remained close to zero ($S_r^- = -0.03$, $S_r^+ = 0.02$), indicating that attenuation was largely insensitive to permeability variations despite substantial changes in infiltration and bank storage.

A non-monotonic behavior of the flow attenuation metrics across the S3 scenarios can be observed, even when maximum bank storage and infiltration fluxes increase systematically with permeability. This behavior likely reflects the fact that maximum bank storage does not necessarily coincide with the flood peak, as bank storage continues to increase after the flood peak has passed. Consequently, the storage volume present near the time of peak discharge is more directly related to attenuation effects than the ultimate maximum storage attained during the event.

Overall, the sensitivity analysis indicates that flood attenuation is controlled primarily by floodplain geometry and flood duration, whereas hydraulic conductivity mainly regulates exchange magnitude and storage development. These findings suggest that attenuation depends not only on total exchange volume but also on the timing of infiltration and subsurface storage evolution.

These findings are derived from an idealized model configuration and should be interpreted as illustrating process behavior rather than providing direct predictions for specific field conditions.

4. Discussion

To improve the physical relevance of the sensitivity analysis, model parameterization and validation were supported using observation-derived bank-storage estimates from the Danube floods of 2013, 2002, and 2006. Agreement between simulated and observation-derived BS_{dry} values, with deviations generally remaining within approximately 31%, indicates that the simplified framework reproduces the order of magnitude of flood-induced groundwater storage beneath the dry floodplain. Nevertheless, model evaluation is based on only three flood events and on groundwater observations located exclusively beneath the dry floodplain, as direct observations beneath inundated floodplains were unavailable. Consequently, the validation provides confidence in the overall representation of flood-induced river–aquifer interactions but does not directly validate the simulated partitioning between vertical floodplain infiltration and horizontal riverbed exchange. The larger validation errors likely reflect uncertainty in the observation-derived estimates arising from sparse groundwater observations, logarithmic extrapolation of groundwater response, and the definition of antecedent groundwater conditions.

The sensitivity analyses indicate that river–aquifer exchange and associated bank storage are jointly controlled by floodplain geometry, flood duration, and subsurface hydraulic properties, which together regulate infiltration intensity, storage development, and flood attenuation. Across all investigated scenarios, the simulations consistently identified vertical floodplain infiltration as the dominant exchange pathway during overbank

flooding, whereas horizontal riverbed exchange remained secondary and progressively approached equilibrium as near-river hydraulic gradients decreased. The reported partitioning between vertical floodplain infiltration and horizontal riverbed exchange should therefore be interpreted as a model-derived estimate rather than a directly validated field observation. However, the persistence of this behavior across the investigated parameter ranges suggests that the predominance of vertical floodplain infiltration is robust within the adopted modeling framework for large alluvial river–floodplain systems.

An important outcome of the sensitivity analysis is that flood duration and floodplain geometry exert control on bank storage and flood attenuation comparable to that of aquifer hydraulic conductivity. While hydraulic conductivity governs the capacity of the subsurface to transmit infiltrated water, flood duration determines the time available for recharge, and floodplain geometry defines the available infiltration area. Consequently, under overbank flood conditions, the simulated magnitude of river–aquifer exchange cannot be interpreted solely in terms of aquifer permeability.

Increasing floodplain width enhanced infiltration by expanding the inundated exchange area. However, the response remained sublinear because wider floodplains reduced overbank flow depth, thereby decreasing the hydraulic head driving infiltration. The subsequent increase in groundwater heads further reduced hydraulic gradients as bank storage developed. The simulated dimensionless indicators further showed that wider floodplains increased the relative importance of vertical infiltration. The relative sensitivity analysis also indicated that flood attenuation responded strongly to changes in floodplain width, with attenuation being more sensitive to floodplain reduction than to equivalent floodplain expansion.

Short-duration floods were characterized by high infiltration fluxes generated by steep hydraulic gradients but by limited storage development because of the short period available for subsurface propagation. In contrast, longer floods sustained infiltration over extended periods, promoting progressive groundwater head rise and larger bank-storage accumulation despite lower instantaneous exchange rates. Relative sensitivity analysis revealed asymmetric attenuation behavior, with strong positive sensitivity for reduced flood duration and negative sensitivity for increased duration. These results indicate that shorter floods enhance instantaneous attenuation through rapid infiltration responses, whereas longer floods favor delayed attenuation through progressive subsurface storage. This decoupling between exchange magnitude and storage is consistent with previous studies of in-bank channel–aquifer interactions [13,40], while extending these interpretations to overbank floodplain systems where infiltration occurs through initially unsaturated floodplain soils.

The simulated response of river–aquifer exchange to subsurface hydraulic properties was nonlinear: substantial increases in hydraulic conductivity produced only moderate gains in storage, except under highly permeable conditions. Relative sensitivity values remained close to zero, indicating that flood attenuation was comparatively insensitive to permeability variations despite noticeable changes in infiltration and storage magnitude. These findings suggest that hydraulic conductivity primarily controls the magnitude of simulated exchange, whereas flood attenuation depends more strongly on floodplain geometry and event duration.

The regime-based framework proposed by Doble et al. [39] provides a useful conceptual interpretation of the simulated results. The consistently high values of the dimensionless recharge indicator F^* indicate that all investigated scenarios operate within a clogging-layer-controlled recharge regime, where the resistance of the riverbed and floodplain clogging layers limits potential recharge more strongly than aquifer storage capacity or transmissivity. Because all investigated cases remain within the same recharge regime,

the indicator primarily identifies the dominant limiting control on recharge rather than explaining differences in bank-storage magnitude among scenarios.

The pathway indicator P^* provides complementary information by quantifying the simulated partitioning between vertical floodplain infiltration and horizontal riverbed exchange during overbank flooding. Unlike F^*, which classifies the dominant recharge regime, P^* characterizes the relative importance of the two exchange pathways within the simulated bank storage. The consistently high simulated P^* values indicate that vertical floodplain infiltration is the dominant exchange pathway throughout the investigated scenarios. Although P^* increases with floodplain width and soil permeability, its decrease with increasing flood duration indicates a relatively larger contribution from horizontal exchange during prolonged events, despite vertical infiltration remaining the dominant pathway. Because P^* is derived directly from the simulated exchange components, it should be interpreted as a diagnostic indicator of the adopted modeling framework rather than as a directly observed field quantity. Furthermore, the indicator is specifically intended for overbank flood conditions. In the absence of floodplain inundation, $BS_V = 0$ by definition, resulting in $P^* = 0$. Consequently, P^* should be interpreted as a descriptor of exchange partitioning during overbank flooding rather than under general river flow conditions.

A complementary perspective is provided by hydrodynamic sensitivity analyses such as Hou et al. [19], which showed that infiltration effects increase with flood duration when evaluated in terms of inundation extent. While this behavior aligns with the present results in terms of increased subsurface storage under longer floods, an important distinction arises from the choice of response variable considered. Inundation-based metrics reflect cumulative water losses over time, whereas discharge and stage hydrographs emphasize the timing and intensity of exchange processes. Consequently, the present results indicate that short-duration floods produce stronger peak discharge attenuation through rapid infiltration responses, mainly associated with rapid vertical floodplain infiltration, whereas longer floods promote attenuation through enhanced bank storage and delayed release. These findings extend previous inundation-focused interpretations by explicitly linking flood attenuation to exchange partitioning and the temporal evolution of subsurface storage during overbank flooding.

The results further highlight the importance of explicitly representing infiltration and bank-storage processes in flood modeling applications. Although calibration of surface-flow parameters such as Manning's roughness coefficient may partially compensate for omitted subsurface exchange when reproducing peak stages or discharges, such adjustments may not reproduce delayed responses associated with temporary subsurface storage [41]. Explicit representation of river–aquifer exchange may therefore improve the physical realism of flood forecasting and flood-risk assessment, particularly in lowland rivers characterized by extensive active floodplains.

The assumption of homogeneous and isotropic subsurface conditions, simplified floodplain geometry, spatially uniform hydraulic properties, and idealized flood hydrographs limits direct transferability to site-specific river systems, where heterogeneous stratigraphy, variable hydraulic connectivity, topographic complexity, and event-specific flood characteristics may substantially modify exchange magnitude and pathway partitioning. These simplifications were intentionally adopted to isolate the first-order controls governing river–aquifer exchange, bank storage, and flood attenuation. Consequently, the results should be interpreted as process-based insights rather than site-specific predictions.

Parameter uncertainty is associated with the selection of hydraulic properties, particularly hydraulic conductivity, which was represented through low-, medium-, and high-conductivity scenarios spanning values reported in the literature. Riverbed conductance was maintained constant throughout the sensitivity analysis because preliminary

simulations indicated a comparatively minor influence under the investigated overbank flood conditions. Consequently, uncertainty associated with riverbed conductance was not explicitly propagated through the sensitivity analyses.

The adopted one-at-a-time sensitivity framework was intentionally selected to isolate the first-order influence of the key parameters on river–aquifer exchange processes. By varying one parameter group while maintaining all others at their benchmark values, the physical mechanisms controlling riverbed exchange, floodplain infiltration, bank storage, and flood attenuation can be interpreted directly without the confounding effects of simultaneous parameter changes.

A limitation of this approach is that it does not explicitly quantify higher-order parameter interactions, parameter equifinality, or correlations among uncertain model parameters, all of which may influence system behavior under specific hydrogeological conditions. Global sensitivity analysis methods would provide additional insight into parameter interactions and the relative importance of uncertain parameters and would therefore represent a natural extension of the present work.

Another limitation relates to the potential for parameter equifinality. The benchmark model was parameterized using representative literature-derived hydraulic properties and evaluated against integrated process indicators, namely observation-derived bank storage beneath the dry floodplain (BS_{dry}), rather than continuous groundwater-head observations. Consequently, different combinations of hydraulic conductivity, riverbed leakance, and hydraulic roughness could potentially reproduce similar integrated responses. Nevertheless, the consistency of the observed sensitivity trends across all investigated scenarios suggests that the principal process-level conclusions are not dependent on a unique parameter combination.

Although the sensitivity analyses consistently identified vertical floodplain infiltration as the dominant exchange pathway across all investigated scenarios, the exact partitioning between vertical floodplain infiltration and horizontal riverbed exchange remains subject to uncertainty. Uncertainties associated with hydraulic parameter estimation, conceptual simplifications (e.g., homogeneous subsurface conditions and idealized floodplain geometry), and the adopted model structure may influence the estimated partitioning between the two exchange pathways. Consequently, the reported values of approximately 82–92% should be interpreted as model-derived estimates for the investigated conditions rather than universal values applicable to all river–floodplain systems.

Future work should extend the framework to heterogeneous floodplain stratigraphy, anisotropic aquifers, spatially variable hydraulic properties, realistic flood hydrographs, and the application of global sensitivity analyses. Additional groundwater observations beneath inundated floodplains would further improve evaluation of the simulated partitioning between vertical and horizontal exchange processes.

5. Conclusions

This study presents a sensitivity analysis of river–aquifer exchange during overbank flooding using a coupled surface water–groundwater framework, with emphasis on the influence of floodplain geometry, flood duration, and subsurface hydraulic properties. The analysis explicitly separated vertical floodplain infiltration and horizontal riverbed exchange and evaluated their contribution to bank storage and flood attenuation.

Model parameterization and validation against Hungarian Danube flood events (2013, 2006, and 2002) reproduced observation-derived bank-storage estimates beneath the dry floodplain within approximately 31%. Although the validation is limited by the availability of field observations and does not directly verify exchange beneath inundated floodplains,

it supports the capability of the modeling framework to reproduce the overall magnitude of flood-induced storage development.

The simulations consistently identified vertical floodplain infiltration as the dominant exchange pathway during overbank flooding, while horizontal riverbed exchange remained secondary. This predominance was observed across all investigated scenarios and was further supported by consistently high values of the pathway indicator (P^*). Because this partitioning is derived from model simulations, it should be interpreted as a model-based estimate for the investigated conditions rather than a field observation.

Floodplain geometry and flood duration exerted influence on bank storage and flood attenuation comparable to, and in several cases greater than, that of aquifer hydraulic conductivity. Wider floodplains enhanced infiltration by increasing the available inundated area, whereas flood duration controlled the balance between rapid infiltration and cumulative storage development. In contrast, hydraulic conductivity primarily influenced the magnitude of river–aquifer exchange but had a comparatively smaller effect on flood attenuation.

Application of the dimensionless recharge indicator (F^*) showed that all investigated scenarios remained within a clogging-layer-controlled recharge regime, indicating that recharge was primarily limited by the resistance of the clogging layer rather than by aquifer storage capacity or transmissivity. Together with P^*, these metrics provide a simple framework for interpreting both the dominant recharge mechanism and the relative importance of the exchange pathways.

Overall, this study extends previous investigations of in-bank river–aquifer interactions by explicitly considering overbank flooding of initially unsaturated floodplains. The proposed framework improves process-based understanding of how floodplain geometry, overbank flood duration, and subsurface permeability jointly regulate river–aquifer exchange, bank storage, and flood attenuation. These findings provide a basis for incorporating physically based river–aquifer interactions into flood modeling and may support future flood-risk assessment and integrated water-resource management in lowland river–floodplain systems.

Author Contributions: Conceptualization, G.d.F.F. and T.K.; Methodology, G.d.F.F. and T.K.; Software, G.d.F.F.; Writing—Original Draft Preparation, G.d.F.F.; Writing—Review and Editing, G.d.F.F. and T.K.; Supervision, T.K.; Funding Acquisition, T.K. All authors have read and agreed to the published version of the manuscript.

Funding: This research was funded by the Ministry of Culture and Innovation and the National Research, Development and Innovation Office, grant number TKP2021-NVA-02.

Data Availability Statement: The original contributions presented in this study are included in the article. Further inquiries can be directed to the corresponding author.

Acknowledgments: This work was carried out with the support of the Stipendium Hungaricum Scholarship Programme, an initiative of the Hungarian Government administered by the Tempus Public Foundation, for which the authors are grateful.

Conflicts of Interest: The authors declare no conflict of interest.

References

1. Pinder, G.F.; Sauer, S.P. Numerical simulation of flood wave modification due to bank storage effects. *Water Resour. Res.* **1971**, *7*, 63–70. [CrossRef]
2. Weng, P.; Sánchez-Pérez, J.M.; Sauvage, S.; Vervier, P.; Giraud, F. Assessment of the quantitative and qualitative buffer function of an alluvial wetland: Hydrological modelling of a large floodplain (Garonne River, France). *Hydrol. Process.* **2003**, *17*, 2375–2392. [CrossRef]

3. Vivoni, E.R.; Bowman, R.S.; Wyckoff, R.L.; Jakubowski, R.T.; Richards, K.E. Analysis of a monsoon flood event in an ephemeral tributary and its downstream hydrologic effects. *Water Resour. Res.* **2006**, *42*. [CrossRef]
4. Derx, J.; Blaschke, A.P.; Blöschl, G. Three-dimensional flow patterns at the river–aquifer interface—A case study at the Danube. *Adv. Water Resour.* **2010**, *33*, 1375–1387. [CrossRef]
5. Liang, X.; Zhan, H.; Schilling, K. Spatiotemporal responses of groundwater flow and aquifer-river exchanges to flood events. *Water Resour. Res.* **2018**, *54*, 1513–1532. [CrossRef]
6. Armoa, O.L.B.; Arnold, J.G.; Bieger, K.; Sauvage, S.; Sánchez-Pérez, J.M. Large wetlands representation in SWAT+: The case of the Pantanal in the Paraguay River Basin. *Front. Water* **2024**, *6*, 1451648. [CrossRef]
7. Bates, P.D.; Stewart, M.D.; Desitter, A.; Anderson, M.G.; Renaud, J.P.; Smith, J.A. Numerical simulation of floodplain hydrology. *Water Resour. Res.* **2000**, *36*, 2517–2529. [CrossRef]
8. Rassam, D.W.; Pagendam, D.E.; Hunter, H.M. Conceptualisation and application of models for groundwater–surface water interactions and nitrate attenuation potential in riparian zones. *Environ. Model. Softw.* **2008**, *23*, 859–875. [CrossRef]
9. Helton, A.M.; Poole, G.C.; Payn, R.A.; Izurieta, C.; Stanford, J.A. Relative influences of the river channel, floodplain surface, and alluvial aquifer on simulated hydrologic residence time in a montane river floodplain. *Geomorphology* **2014**, *205*, 17–26. [CrossRef]
10. Bernard-Jannin, L.; Brito, D.; Sun, X.; Jauch, E.; Neves, R.; Sauvage, S.; Sánchez-Pérez, J.M. Spatially distributed modelling of surface water-groundwater exchanges during overbank flood events-a case study at the Garonne River. *Adv. Water Resour.* **2016**, *94*, 146–159. [CrossRef]
11. Morin, E.; Grodek, T.; Dahan, O.; Benito, G.; Kulls, C.; Jacoby, Y.; Van Langenhove, G.; Seely, M.; Enzel, Y. Flood routing and alluvial aquifer recharge along the ephemeral arid Kuiseb River, Namibia. *J. Hydrol.* **2009**, *368*, 262–275. [CrossRef]
12. Doppler, T.; Franssen, H.J.H.; Kaiser, H.P.; Kuhlman, U.; Stauffer, F. Field evidence of a dynamic leakage coefficient for modelling river–aquifer interactions. *J. Hydrol.* **2007**, *347*, 177–187. [CrossRef]
13. Chen, X.; Chen, X. Stream water infiltration, bank storage, and storage zone changes due to stream-stage fluctuations. *J. Hydrol.* **2003**, *280*, 246–264. [CrossRef]
14. McDonald, M.G.; Harbaugh, A.W. *A Modular Three-Dimensional Finite-Difference Ground-Water Flow Model (Open-File Report 83–875)*; U.S. Geological Survey, Techniques of Water-Resources Investigations: Reston, VA, USA, 1988. [CrossRef]
15. Harbaugh, A.W. MODFLOW-2005: The U.S. Geological Survey modular ground-water model—The ground-water flow process. In *U.S. Geological Survey Techniques and Methods 6-A16*; US Department of the Interior, US Geological Survey: Reston, VA, USA, 2005; p. 6-A16. [CrossRef]
16. Niswonger, R.G.; Prudic, D.E. Documentation of the Streamflow-Routing (SFR2) Package to include unsaturated flow beneath streams—A modification to SFR1 (Version 1.2, revised Aug 2009). In *U.S. Geological Survey Techniques and Methods 6-A13*; US Department of the Interior, US Geological Survey: Reston, VA, USA, 2005. [CrossRef]
17. Graham, D.N.; Butts, M.B. Flexible, integrated watershed modelling with MIKE SHE. In *Watershed Models*; Singh, V.P., Frevert, D.K., Eds.; CRC Press, Taylor & Francis: Boca Raton, FL, USA, 2005; pp. 245–272, ISBN 0849336090.
18. Brunner, P.; Simmons, C.T. HydroGeoSphere: A Fully Integrated, Physically Based Hydrological Model. *Groundwater* **2012**, *50*, 170–176. [CrossRef]
19. Hou, J.; Zhang, Z.; Zhang, D.; Shi, B.; Chen, G.; Zhang, H. Study on the influence of infiltration on flood propagation with different peak shape coefficients and duration. *Water Policy* **2021**, *23*, 1059–1074. [CrossRef]
20. Rassam, D.W.; Pickett, T.; Knight, J.H. Incorporating floodplain groundwater interactions in river modelling. In Proceedings of the 18th World IMACS/MODSIM Congress, Cairns, Australia, 13–17 July 2009; pp. 3116–3122.
21. Costa, A.C.; Bronstert, A.; de Araujo, J.C. A channel transmission losses model for different dryland rivers. *Hydrol. Earth Syst. Sci.* **2012**, *16*, 1111–1135. [CrossRef]
22. Ferraz, G.F.; Krámer, T. A simple mechanistic coupled surface–groundwater model to evaluate bank storage and flood attenuation in lowland rivers. *Period. Polytech. Civ. Eng.* 2026, *accepted*. [CrossRef]
23. Chaudhry, M.H. Governing equations for one-dimensional flow. In *Open-Channel Flow*; Springer: Boston, MA, USA, 2008. [CrossRef]
24. Rashid, R.M.; Chaudhry, M.H. Flood routing in channels with flood plains. *J. Hydrol.* **1995**, *171*, 75–91. [CrossRef]
25. Freeze, R.A.; Cherry, J.A. *Groundwater*; Prentice-Hall: Englewood Cliffs, NJ, USA, 1979.
26. Green, W.H.; Ampt, G.A. Studies on soil physics: Flow of air and water through soils. *J. Agric. Sci.* **1911**, *4*, 1–24. [CrossRef]
27. Kale, R.V.; Sahoo, B. Green-Ampt infiltration models for varied field conditions: A revisit. *Water Resour. Manag.* **2011**, *25*, 3505–3536. [CrossRef]
28. Doble, R.; Brunner, P.; McCallum, J.; Cook, P.G. An analysis of river bank slope and unsaturated flow effects on bank storage. *Groundwater* **2012**, *50*, 77–86. [CrossRef] [PubMed]
29. Rassam, D.W. A conceptual framework for incorporating surface–groundwater interactions into a river operation–planning model. *Environ. Model. Softw.* **2011**, *26*, 1554–1567. [CrossRef]

30. Liang, X.; Zlotnik, V.A.; Zhang, Y.K.; Xin, P. Diagnostic analysis of bank storage effects on sloping floodplains. *Water Resour. Res.* **2020**, *56*, e2019WR026385. [CrossRef]
31. Gábris, G.; Pécsi, M.; Schweitzer, F.; Telbisz, T. Relief. In *National Atlas of Hungary: Natural Environment*; Kocsis, K., Ed.; Hungarian Academy of Sciences Centre for Astronomy and Earth Sciences Geographical Institute: Budapest, Hungary, 2018; pp. 42–57.
32. Sztanó, O.; Kováč, M.; Magyar, I.; Šujan, M.; Fodor, L.; Uhrin, A.; Rybár, S.; Csillag, G.; Tőkés, L. Late Miocene sedimentary record of the Danube/Kisalföld Basin: Interregional correlation of depositional systems, stratigraphy and structural evolution. *Geol. Carpathica* **2016**, *67*, 525–542. [CrossRef]
33. Trásy, B.; Magyar, N.; Havril, T.; Kovács, J.; Garamhegyi, T. The role of environmental background processes in determining groundwater level variability: An investigation of a record flood event using dynamic factor analysis. *Water* **2020**, *12*, 2336. [CrossRef]
34. Calver, A. Riverbed permeabilities: Information from pooled data. *Groundwater* **2001**, *39*, 546–553. [CrossRef] [PubMed]
35. Wu, C.; Lu, C.; Chen, J.; Liu, J.; Zhang, H.; Saidy, E.; Shu, L. Spatio-temporal variability of hydraulic conductivity in the floodplain riverbank of a hyporheic zone. *Catena* **2023**, *228*, 107172. [CrossRef]
36. Ubell, K. Surface- and ground-water relationships along the Hungarian reach of the Danube River. *Internat. Assoc. Sci. Hydrol. Pub.* **1964**, *63*, 502–512.
37. Anderson, M.P.; Woessner, W.W.; Hunt, R.J. *Applied Groundwater Modeling: Simulation of Flow and Advective Transport*; Academic Press: Cambridge, MA, USA, 2015.
38. Hamby, D.M. A review of techniques for parameter sensitivity analysis of environmental models. *Environ. Monit. Assess.* **1994**, *32*, 135–154. [CrossRef] [PubMed]
39. Doble, R.C.; Crosbie, R.S.; Smerdon, B.D.; Peeters, L.; Cook, F.J. Groundwater recharge from overbank floods. *Water Resour. Res.* **2012**, *48*, W09522. [CrossRef]
40. Siergieiev, D.; Ehlert, L.; Reimann, T.; Lundberg, A.; Liedl, R. Modelling hyporheic processes for regulated rivers under transient hydrological and hydrogeological conditions. *Hydrol. Earth Syst. Sci.* **2015**, *19*, 329–340. [CrossRef]
41. Saksena, S.; Merwade, V.; Singhofen, P.J. Flood inundation modelling and mapping by integrating surface and subsurface hydrology with river hydrodynamics. *J. Hydrol.* **2019**, *575*, 1155–1177. [CrossRef]

Disclaimer/Publisher's Note: The statements, opinions and data contained in all publications are solely those of the individual author(s) and contributor(s) and not of MDPI and/or the editor(s). MDPI and/or the editor(s) disclaim responsibility for any injury to people or property resulting from any ideas, methods, instructions or products referred to in the content.